MADRID
inter.noise 2019
June 16 - 19
NOISE CONTROL FOR A BETTER ENVIRONMENT

Investigation of installation effect of jet noise from turbofan engines

Zhang, Yingzhe[1], Lin, Dakai[2], Yang, Zhigang[3], and Lee, Incheol[4],
Beijing Aeronautical Science and Technology Research Institute of COMAC,
Beijing Key Laboratory of Simulation Technology for Civil Aircraft Design
China North of Future Science Park, Changping District Beijing, 102211 P. R. China

ABSTRACT

To quantitatively investigate the impact of installation on jet noise from modern high bypass ratio (BPR) turbofan engines, a model-scale noise experiment with a jet propulsion system and a realistic fuselage model was conducted in the anechoic wind tunnel of ONERA, CEPRA 19. Two area ratios (an area of the secondary nozzle over an area of the primary nozzle), 5 and 7, and various airframe configurations such as positions relative to the jet nozzle position and flap angles, were considered. The followings were investigated using the acoustic data acquired from the experiment: (1) impact of the presence of the airframe; (2) impact of flap angles; (3) impact of jet nozzle position relative to the wing; and (4) flight effect. Based on the observation, it could be concluded that the frequency region can be divided into two parts: the low frequencies (≤ 1.5 kHz) and high frequencies (> 1.5 kHz). It seems that the interaction between the jet and the pressure side of the wing contributes the noise at the low frequencies and the interaction between the jet and the flap tip contributes the noise at the high frequencies.

Keywords: Installation effect, Jet noise, Jet flap interaction, Turbofan engine
I-INCE Classification of Subject Number: 74

1. INTRODUCTION

When turbo-fan engines are installed on an airplane, typically underneath the wing, the flow/acoustic interactions between them change considerably. Such interactions due to engine installation could be defined as jet engine interactions, and these interactions have become an important and fast-growing area in aeroacoustics research. The change in the flow/acoustic field can arise, for example, the reflection and diffraction of engine noise by the wing and its high-lift devices such as flaps, or the interaction of the exhaust jet and flaps that can generate new noise sources, which is also well known as jet-flap interaction (JFI) noise[0]. It has been known that the flap deflection angle, the distance between the jet and the wing structure, and the jet velocity are the three critical parameters for JFI noise.

[1] zhangyingzhe@comac.cc
[2] lindakai@comac.cc
[3] yangzhigang1@comac.cc
[4] incheol.lee2@gmail.com

When an airplane approaches, the flaps are deployed considerably, but the jet velocity of the engines is low. Whereas, at take-off conditions, the flaps are not deployed as much, but the jet velocity is high. Hence, it is important to study JFI noise at both approach and take-off conditions although traditionally airframe/fan noise and jet/fan noise are considered dominant sources of noise at those two conditions respectively[0].

For under the wing configurations, Fink[0] proposed that there would be three mechanisms for the jet-flap interaction noise. For under the wing configurations: (1) lift fluctuation noise, (2) trailing edge noise, and (3) quadrupole noise from the deflected flap. The common feature in all of them is that they radiate noise predominantly in the front quadrant due to the deflection of the flap. When the flaps are not completely immersed in the jet stream, the JFI noise may be treated as a noise source. Although all the above mechanisms have some relevance to JFI noise, the most important one would be the trailing edge noise mechanism where the convection of turbulent eddies across the trailing edge of the flap generates noise.

Trailing edge noise has been studied quite thoroughly in the literature by Howe[0] and by Crighton[0]. There has been a variety of experimental work to analyze both jet-wing interaction noise and jet-flap interaction noise. For instance, Sengupta[0] analyzed the impact of the wing part without flap deflection and is modeled in terms of lift fluctuation noise, trailing edge noise, and jet noise reflection. He defined the JFI noise as the additional component purely due to flap deflection and is modeled in terms of lift fluctuations on the flaps diffracted by the wing trailing edge. The effect of engine strut height, flap cut-out and porous extension to the trailing edge of flaps on JFI noise were studied parametrically. Brown and Ahuja[0] investigated the mid-frequency hump in the front quadrant in their noise data to JFI noise and analyzed the effect on it due to a systematic variation of flap parameters, such as flap angle, flap cut-out, the angle of attack, and location of the jet with respect to the wing, and jet velocity. Elkoby[0] has studied the issue of propulsion airframe aeroacoustic interactions, which includes JFI as a component, at full scale by examining the differences between flight test data and static engine test data projected to flight test conditions without the installation effects. These spectral differences at full scale were not always explainable although they matched the trends from model tests. Mengle[0] studied JFI noise as well as the attachment of jet flow to the wing in a model-scale wind tunnel test. He verified that the decrease in gulley height and increase in flap angle leads to higher installed noise. He found that at smaller gulley heights and larger flap angles, there appear, not one, but two distinct peak noise frequencies in the front quadrant and they merge into each other as the emission angle goes towards the jet axis. Even recently, there have been many investigations on the noise induced by the engine installation underneath the wing[0-0]. Jordan et al.[0] investigated the tonal noise generated by JFI. They observed that the distribution of spectral peaks couldn't be explained using the usual edge-tone model, in which resonance is underpinned by coupling between downstream-traveling Kelvin–Helmholtz wave packets and upstream-traveling sound waves. As introduced above, there have been many works, mainly experimentally, to understand the characteristics of noise induced by the jet-wing interaction. However, the investigation of jet engine installation noise has been still an exciting and complicated challenge.

A model-scale noise test was carried out in the anechoic wind tunnel of ONERA, CEPRA19. A realistic swept wing-fuselage model and a couple of dual nozzle models were used in the test to investigate the jet noise from aircraft engines for isolated configurations as well as for installed configurations. In this paper, the data of the installed configurations were investigated to understand the characteristics of noise induced by engine wing installation.

2. TEST INFORMATION

2.1 Test facility and measurement system

The acoustic test was carried out in the anechoic wind tunnel of ONERA, CEPRA 19, where various types of acoustic measurement including jet noise have been carried out. Figure 1 shows an overview of the interior of the tunnel with an installed dual nozzle configuration. The chamber is roughly a quarter of a sphere with an internal radius of 9.6m. The flight stream for wind-on nozzle-operating conditions is provided through a 2m diameter nozzle, and the maximum flow speed is 130m/s. There are two arc-shaped arrays installed in the tunnel as shown in Figure 1; one is defined as "flyover array", and the other is defined as "sideline array". The diameter of the two arrays is 6m, and the reference is set to the center of the exit plane of the fan nozzle. The flyover array covers the geometrical angles from 40 to 160 degrees with 13 high-performance microphones, whereas the sideline array covers the geometrical angles from 40 to 150 degrees with high-performance 12 microphones. The two arrays were designed to observe the detailed noise characteristics of the jet noise with an airframe model installed. Therefore, there would be no difference in spectra measured by the two arrays for the isolated configurations theoretically. The nozzles were attached to the CEPRA 19 nozzle rig (SMT2), which provides the primary and the secondary flows at requested nozzle operation conditions. The maximum combined mass flow (primary flow and secondary flow) is about 12kg/sec, and the rig could cover all the nozzle-operating conditions defined in the test matrix including extremely high-temperature conditions.

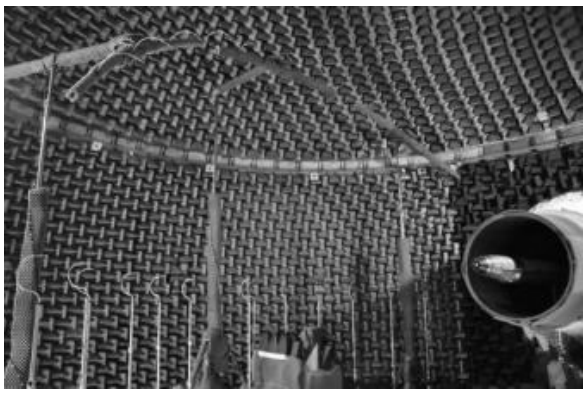

Figure 1 Anechoic wind tunnel in ONERA (CEPRA 19)

2.2 Test models

Various configurations of nozzles for dual-stream jet and an airframe in model-scale were designed and manufactured to investigate the characteristics of noise generated by isolated configurations as well as installed configurations. As described earlier, two kinds of area ratios, 5 (AR5) and 7 (AR7), were selected to cover a wide range of area ratios that are corresponding to a turbofan engine of both the current generation and the next generation. And these area ratios can cover the BPR (bypass ratio) up to 14 depending on nozzle-operating conditions. The size of the fan nozzle of which diameter at the exit plane is 168 mm was kept consistent regardless of the area ratios. Two different plugs where manufactured while keeping the same core and fan nozzles. Figure 2 shows a photo of nozzle tested in CEPRA 19.

An airframe with detailed design was tested as shown in Figure 3.The wing part and fuselage were scaled from an aircraft but cut short to keep the model in the tunnel jet flow and to minimize unwanted interaction between the shear layer of the tunnel and the fuselage structure. No pylon structure was attached between the nozzle and the wing. This enabled the experiment to be very

Figure 2 A nozzle installed on the jet rig

efficient since significant time was not consumed due to a model change when the position of the wing changed.

Figure 3 Photos of the airframe model

2.3 Nozzle-operating conditions

The jet flow from a dual nozzle is characterized by a host of parameters: NPR_P, NTR_P, NPR_S, NTR_S, and AR. The subscripts P and S denote primary (core) and secondary (fan) streams, respectively. All the aerodynamic values used for the definition of the parameters are total pressure and total temperature values. The noise from a dual-stream nozzle is dependent on the above thermodynamic and geometric parameters.

More than 20 nozzle-operating conditions were defined to achieve the noise characteristics of both systematically varying nozzle-operating conditions and realistic engine operating conditions. Table 1**Error! Reference source not found.** shows a part of the systematically varying conditions. Due to limited space, the results of two conditions that simulate an actual approach condition (NOC1) and a take-off condition (NOC2) are mainly presented in this paper. Five tunnel Mach numbers, M = 0.00, 0.10, 0.20, 0.25, and 0.30, were defined. It should be noted that the highest Mach number was tested only for the conditions of extremely high-power settings due to intensive background noise.

Table 1 Part of nozzle-operating conditions

Primary nozzle		Secondary nozzle	
Temperature ratio (NTR_P)	Pressure ratio (NPR_P)	Temperature ratio (NTR_S)	Pressure ratio (NPR_S)
1.300	2.400	1.500	1.000
1.500	2.700	1.700	1.000
1.700	3.200	1.850	1.000
1.850	3.200	1.850	1.000

2.4 Airframe configurations

4 flap angles, 0, 19, 25, and 34 degrees, were defined. And the relative position of the wing part in the direction of the jet stream (x) and in the vertical direction (y) was defined as introduced in Figure 1.

The critical length parameters related to the installation noise are introduced in Figure 50. Since the jet flow and the shear layer of the secondary flow is supposed to directly interact with the wing structures such as the pressure side of the wing and the flap, all parameters are non-dimensionalized by the radius of the secondary nozzle at the nozzle exit, R_{sec}. Table 2 to Table *6* show the parameters for different flap angles and airframe positions.

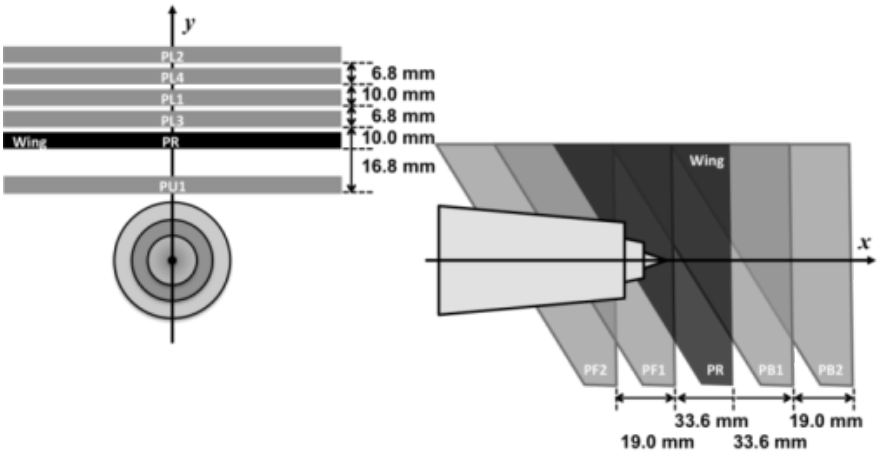

Figure 4 Schematic drawing of the positions of airframe relative to the jet nozzle

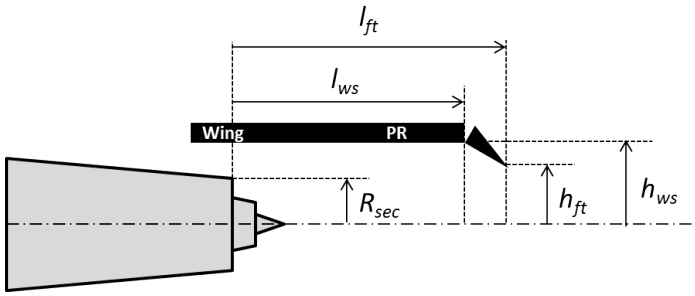

Figure 5 Definition of length parameters

Table 2 Length parameters with the airframe positioned at PR

	PR, Flap0	PR, Flap19	PR, Flap25	PR, Flap34
h_{ws}/R_{sec}	1.12	1.12	1.12	1.12
h_{ft}/ R_{sec}	1.47	0.84	0.69	0.48
l_{ws}/ R_{sec}	4.08	4.64	4.64	4.64
l_{tf}/ R_{sec}	5.65	6.12	6.05	5.93

Table 3 Length parameters with the flap at 0 degrees

	PU1, Flap0	PL3, Flap0	PL1, Flap0	PL4, Flap0	PL2, Flap0	PF2, Flap0	PF1, Flap0	PB1, Flap0	PB2, Flap0
hws/Rsec	0.92	13.22	1.32	1.44	1.52	1.12	1.12	1.12	1.12
hft/ Rsec	1.15	1.47	1.55	1.67	1.75	0.84	0.84	0.84	0.84
lws/ Rsec	4.08	4.08	4.08	4.08	4.08	4.71	4.48	3.68	3.46
ltf/ Rsec	5.65	5.65	5.65	5.65	5.65	6.27	6.05	5.25	5.02

Table 4 Length parameters with the flap deployed to 19 degrees

	PU1, Flap19	PL3, Flap19	PL1, Flap19	PL4, Flap19	PL2, Flap19	PF2, Flap19	PF1, Flap19	PB1, Flap19	PB2, Flap19
h_{ws}/R_{sec}	0.92	1.24	1.32	1.44	1.52	1.12	1.12	1.12	1.12
h_{ft}/ R_{sec}	0.64	0.96	1.04	1.16	1.24	0.84	0.84	0.84	0.84
l_{ws}/ R_{sec}	4.64	4.64	4.64	4.64	4.64	5.26	5.04	4.24	4.01
l_{tf}/ R_{sec}	6.12	6.12	6.12	6.12	6.12	6.74	6.52	5.72	5.49

Table 5 Length parameters with the flap deployed to 25 degrees

	PU1, Flap25	PL3, Flap25	PL1, Flap25	PL4, Flap25	PL2, Flap25	PF2, Flap25	PF1, Flap25	PB1, Flap25	PB2, Flap25
h_{ws}/R_{sec}	0.92	1.24	1.32	1.44	1.52	1.12	1.12	1.12	1.12
h_{ft}/R_{sec}	0.49	0.81	0.89	1.01	1.09	0.69	0.69	0.69	0.69
l_{ws}/R_{sec}	4.64	4.64	4.64	4.64	4.64	5.26	5.04	4.24	4.01
l_{tf}/R_{sec}	6.12	6.05	6.05	6.05	6.05	6.68	6.45	5.65	5.43

Table 6 Length parameters with the flap deployed to 34 degrees

	PU1, Flap34	PL3, Flap34	PL1, Flap34	PL4, Flap34	PL2, Flap34	PF2, Flap34	PF1, Flap34	PB1, Flap34	PB2, Flap34
h_{ws}/R_{sec}	0.92	1.24	1.32	1.44	1.52	1.12	1.12	1.12	1.12
h_{ft}/R_{sec}	0.28	0.59	0.68	0.79	0.88	0.48	0.48	0.48	0.48
l_{ws}/R_{sec}	4.64	4.64	4.64	4.64	4.64	5.26	5.04	4.24	4.01
l_{tf}/R_{sec}	5.93	5.93	5.93	5.93	5.93	6.56	6.33	5.53	5.31

3. RESULTS AND DISCUSSION

Measured noise data were investigated under four subjects: the presence of airframe, airframe position, flap angles, and flight effect. Each figure in the following section shows the spectral comparison at 4 angles: 60, 80, 100, and 130 degrees for the observation of the installation effect. Note that corrections due to atmospheric absorption, microphone's frequency response, and shear layer correction were applied to the data.

3.1 Impact of airframe presence

Figure 6 and Figure 7 show the comparison between the spectra with the airframe and without the airframe at two nozzle-operating conditions, NOC1 and NOC2, for two area ratios. In each figure, the spectra have been spaced apart to enhance visual observation. The flap angle was set to 0 degrees when installed under the wing.

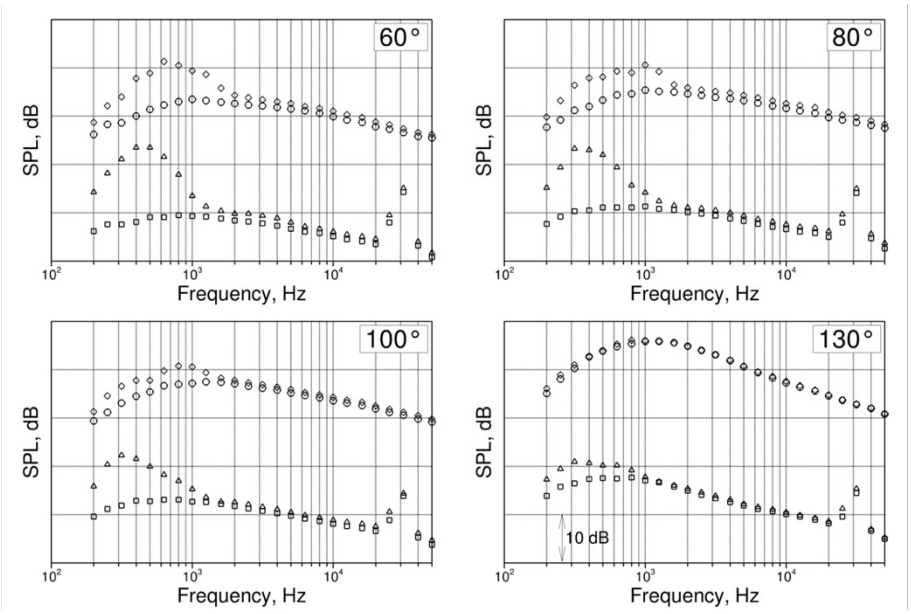

Figure 6 Effect of airframe presence (AR5, flap @ 0 degrees, $M_T = 0$; □: NOC1, isolated; △: NOC1, airframe @ PR; ○: NOC2, isolated; and ◇: NOC2, airframe @ PR)

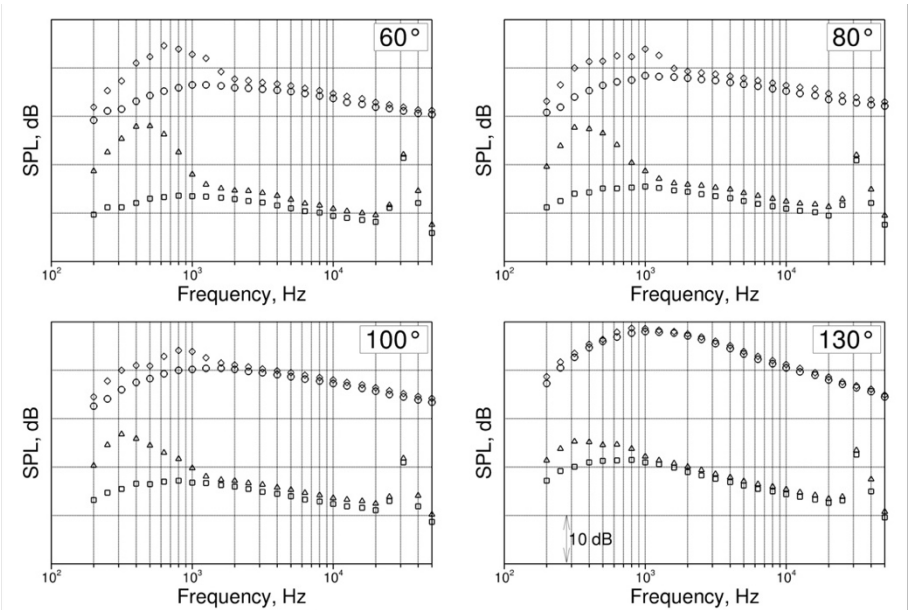

Figure 7 Effect of airframe presence (AR7, flap @ 0 degrees, $M_T = 0$; □: NOC1, isolated; ∆: NOC1, airframe @ PR; ○: NOC2, isolated; and ◇: NOC2, airframe @ PR)

The followings are the key findings from the data. Distinct broad humps are observed at forward angles, and the hum is diminished as the angle increases. The hump is more pronounced at NOC1 than at NOC2. This trend is observed because the effect of the presence of the airframe is pronounced by the interaction between the jet flows, mainly the secondary flow, and the wing structure. And the spreading rate of the jet flow is inversely proportional to the pressure ratio: the jet flow of NOC1 has the higher spreading ratio though the absolute velocity is low, and this induced more interaction between the jet and the surface of the wing. No clear trend is observed at aft angles, and no distinct difference is observed between the two area ratios either.

3.2 Impact of airframe position

Figure 8 and Figure 9 show the spectral comparison of various positions of the wing model in the vertical direction relative to the jet nozzle at the take-off condition (NOC2). It is observed that the spectra change at the low frequency up to 1.5 kHz when the airframe moved in the vertical direction when the flap angle is set to 0 degrees. The spectral change is more pronounced at forward angles than at aft angles. When the flap is deployed, the broadband component of spectra changes significantly at the frequency higher than 1.5 kHz and the change is also observed at the aft angle, 130 degrees. A tonal component at 1.5 kHz is also pronounced when the jet and the airframe get closer, and the strength of the tone reduces as the angle increases. The difference of configurations between Figure 8 and Figure 9 is the flap angle: 0 and 25 degrees. Thus, the spectral variation at around 1 kHz observed in Figure 8 is linked to the interaction between the jet stream and the pressure side of the wing and the spectral variation at mid-to-high frequencies is linked to the interaction between the jet stream and the flap.

Figure 10 shows the spectral comparison of various positions of the wing model in the jet-flow direction relative to the jet nozzle at NOC2. It is clearly observed that the spectral change due to the airframe position in the jet-flow direction is limited. This trend is almost consistent regardless of the power setting and flap angles. It is interesting to observe that the noise decreased as the distance

between the nozzle exit and the trailing edge of the flap decreased, and vice versa, at forward angles. Before conducting the experiment, the noise of the airframe at PB2 was expected to be lower than that of the airframe at PF2, since the noise was inversely proportional to the distance between the noise source and the interaction point as observed in Figure 9. However, the actual measurement was contrary to the expectation, and the trend of spectral change is very similar to the trend observed in Figure 8, meaning the spectral variation due to the airframe position in the jet-flow direction is related to the pressure side of the wing rather than the tip of the flap.

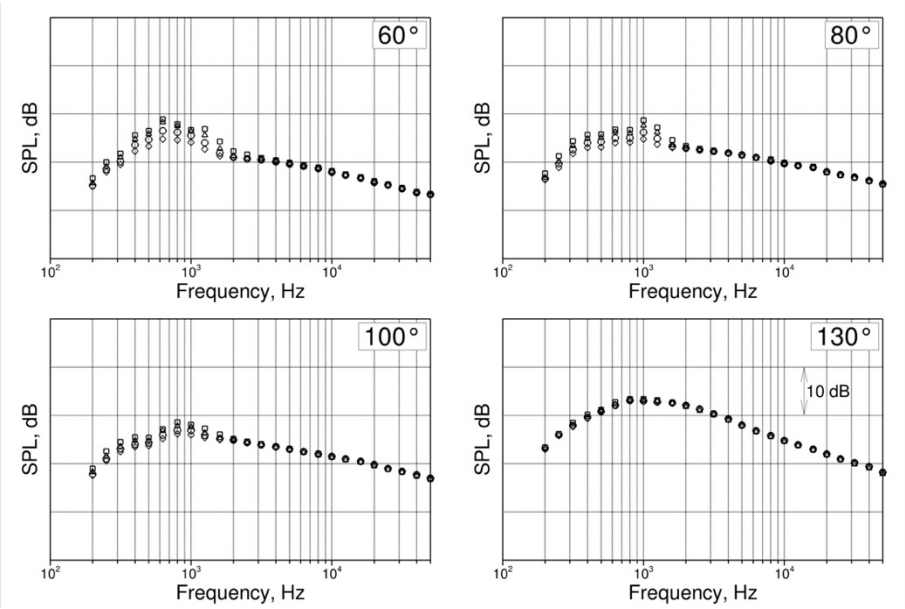

Figure 8 Effect of airframe positions in the vertical direction (AR5, flap @ 0 degrees, NOC2, $M_T = 0$; □: PU1; △: PR; ○: PL1; and ◇: PL2)

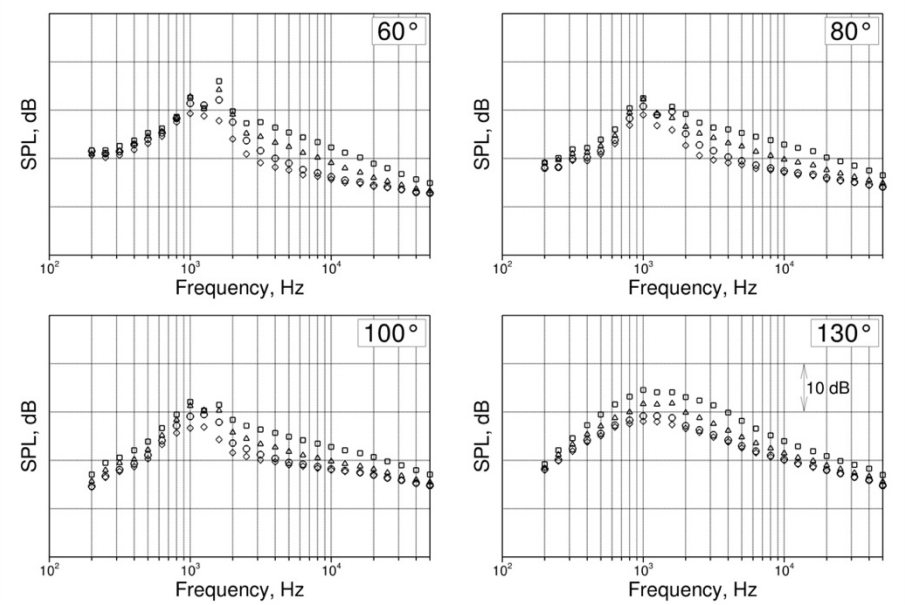

Figure 9 Effect of airframe positions in the vertical direction (AR5, flap @ 25 degrees, NOC2, $M_T = 0$; □: PU1; △: PR; ○: PL1; and ◇: PL2)

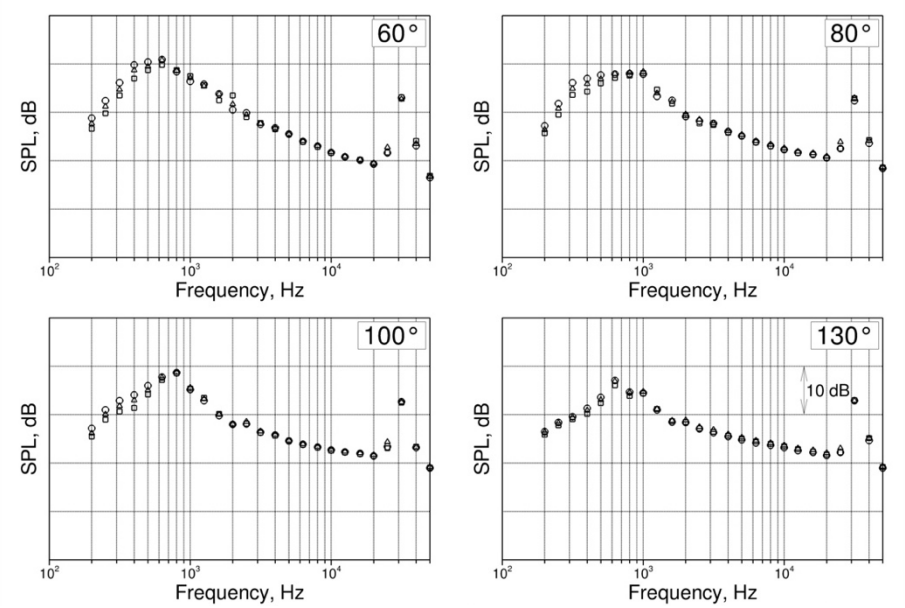

Figure 10 Effect of airframe positions in the jet-flow direction (AR7, flap @ 19 degrees, NOC2, M_T = 0.1; □: PF2; △: PR; and ○: PB2)

3.3 Impact of flap angle

The spectral comparisons of various flap angles at the approach (NOC1), and take-off (NOC2) conditions are shown in Figure 11 and Figure 12 respectively. It should be noted that the spectra of the wing configuration without the flap part (□) is compared to the spectra of the configurations of various flap settings. The data shows that at NOC2, there exist a hump at the forward angles and it becomes strong as the flap angle increases. And it reduces as the angle increases. Also, the number of peaks of the hump is 2 at some of the forward angles. Note that there exists a tonal component at 30 kHz which is independent of the flap angle at NOC1. The tonal noise is supposed to be generated because the velocity of the primary and secondary streams is close. Though the noise seems to be substantial, it was not audible because its frequency is too high.

Based on the observation in the previous section, it is worth to divide the frequency region into two parts: the low frequencies (≤ 1.5 kHz) and high frequencies (> 1.5 kHz). The increase of broadband component at the mid-to-high frequency is more pronounced. At the low frequencies, the spectrum increases when the flap is deployed. However, there is no substantial difference between 25 and 34 degrees at NOC1 and 19 and 25 degrees at NOC2 at the low frequencies. The minimum distance from the jet center to the tip of the flap (h_{fl}/R_{sec}) is 1.47 for the undeployed flap and 0.84, 0.69, and 0.48 for the flap at 19, 25, and 34 degrees respectively according to Table 2. Thus, the tip of the flap is located inside the jet stream for all deployed flaps, and no significant spectral change is expected when the location of the flap tip changes inside the jet stream. It is interesting to observe that the presence of the flap part has an impact on the low frequencies, which means it is related to the interaction between the jet and the pressure side of the wing.

At the high frequencies, it is observed that there exists a boost of the broadband component as a function of the flap angle and it becomes small as the frequency increases. This trend is more pronounced at forward angles than aft angles and at the approach condition than at the take-off condition.

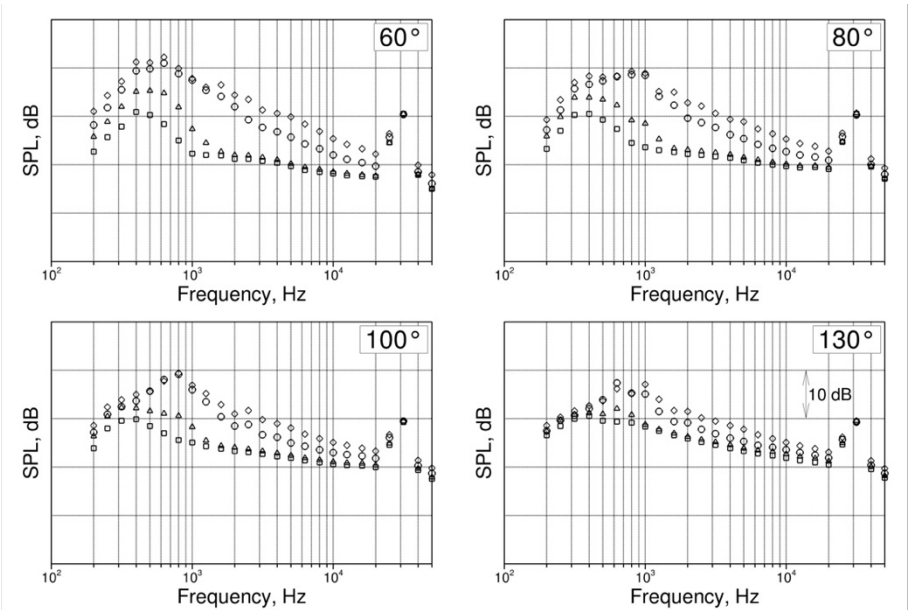

Figure 11 Effect of flap angles (AR5, airframe @ PR, NOC1, M_T = 0.2; □: flap removed; △: flap @ 0 degrees; ○: flap @ 25 degrees; and ◇: flap @ 34 degrees)

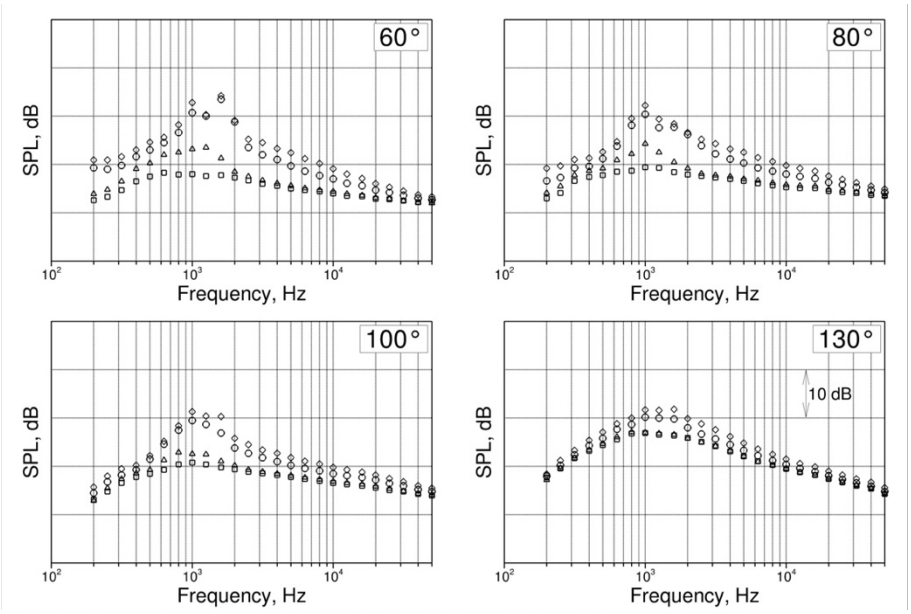

Figure 12 Effect of flap angles (AR5, airframe @ PR, NOC2, M_T = 0.2; □: flap removed; △: flap @ 0 degrees; ○: flap @ 19 degrees; and ◇: flap @ 25 degrees)

3.4 Flight effect

In reality, the noise of an airplane actually does matter when it flies in the sky. Thus, it is necessary to consider the effect of flight or the effect of free streams of the wind tunnel. During the experiment, the effect of free streams was briefly investigated at various nozzle-operating conditions. As mentioned at the beginning of section 3, the shear layer correction was applied to the wind-on data. Figure 13 shows the effect of free streams which vary from a Mach number of 0 to 0.25 at a nozzle-operating condition close to the mid-power setting of an actual turbofan engine. It is clearly observed that the spectral difference between the static condition and the condition of the maximum tunnel speed (M_T = 0.25) is about 7 dB at forward angles and 9 dB at aft angles. The flight effect gets reduced as the frequency increases at certain angles, mostly forward angles.

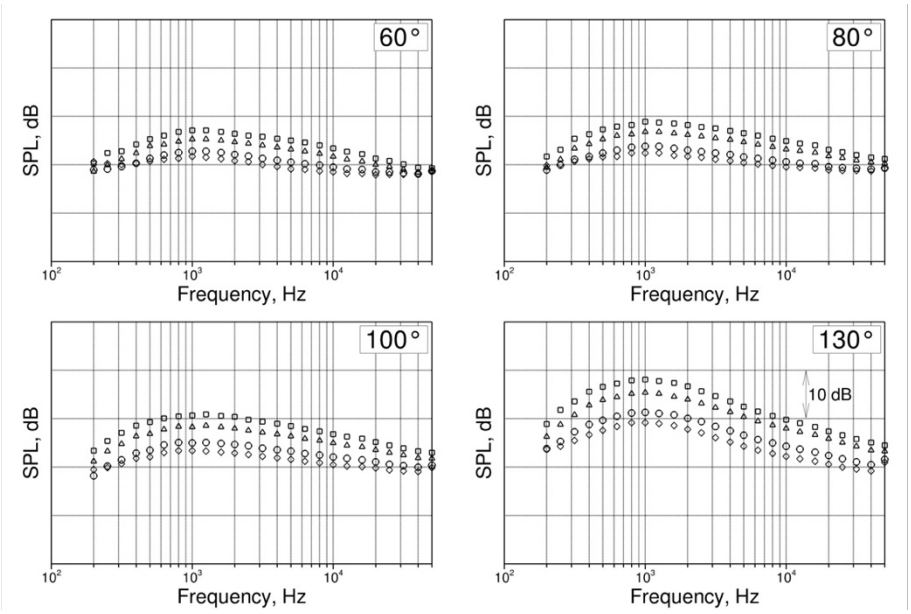

Figure 13 Flight effect (AR5, airframe @ PR, NPR_P = 1.317, NTR_P = 2.630, NPR_S = 1.500, NTR_S = 1.000; □: M_T = 0; △: M_T = 0.1; ○: M_T = 0.2; and ◇: M_T = 0.25)

4. CONCLUSIONS

Most of the modern commercial aircraft has its turbofan engines installed under the wing. It has been well known that the jet noise from a turbofan engine installed under the wing is more significant than the jet noise from an isolated turbofan engine due to installation effect. To quantitatively investigate the impact of installation on jet noise from modern high BPR turbofan engines, authors carried out a model-scale noise experiment with a jet propulsion system and a realistic fuselage model at the anechoic wind tunnel of ONERA, CEPRA 19. Two area ratios (an area of the secondary nozzle over an area of the primary nozzle), 5 and 7, and various airframe were considered to investigate the installed jet noise such as impact of the presence of an airframe, impact of flap angles, and impact of an airframe position relative to the jet nozzle. The flight effect is also briefly investigated.

When there exists an airframe, distinct broad humps are observed at forward angles, and the hum is diminished as the angle increases. The hump is more pronounced at the approach condition than at the take-off condition. When the airframe moves in the vertical direction, the spectra change at the low frequency up to 1.5 kHz especially at forward angles for the undeployed flap and, the spectra change significantly at the frequency higher than 1.5 kHz for the deployed flaps. The spectral change is limited when the airframe moves in the jet-flow direction. When the flap is deployed, a hump of which peak frequency is a function of a nozzle-operating condition and a flap angle shows up at the forward angles. The spectral difference between the static condition and the condition of the maximum tunnel speed (MT = 0.25) is about 7 dB at forward angles and 9 dB at aft angles.

5. ACKNOWLEDGEMENTS

The authors thank Mr. Zhi Deng of BASTRI for his support for the successful execution of the experiments. The support of the project management team for the project successfully execution is appreciated. The support of staff at CEPRA 19 of ONERA for scheduling and conducting the test, and maintaining the facility is also appreciated.

6. REFERENCES

1. Fink, M. R., "Propulsive Lift Noise," Aeroacoustics of Flight Vehicles: Theory and Practice, Volume 1: Noise Sources, edited by Hubbard, H.H., NASA Ref. Publication 1258, Vol. 1, Ch. 8, Aug. 1991.

2. Groeneweg, J. F., Sofrin, T. G., Rice, E. J. and Gliebe, P. R., "Turbomachinery Noise," Aeroacoustics of Flight Vehicles: Theory and Practice, Volume 1: Noise Sources, edited by Hubbard, NASA Ref. Publication 1258, Vol. 1, Ch. 3, Aug. 1991.

3. Howe, M. S., "A Review of the Theory of Trailing Edge Noise," J. Sound & Vibration, vol. 61, no. 3, Dec. 8, 1978, pp. 437- 465

4. Crighton, D. G., "Airframe Noise," Aeroacoustics of Flight Vehicles: Theory and Practice, Volume 1: Noise Sources, edited by Hubbard, H.H., NASA Ref. Publication 1258, Vol. 1, Ch. 7, Aug. 1991.

5. Sengupta, G., "Analysis of Jet-Airframe Interaction Noise," 8th Aeroacoustics Conference, AIAA 83-0783, 1983.

6. Brown, W. H., and Ahuja, K. K., "Jet and Wing/Flap Interaction Noise," AIAA 84-2362, 1984.

7. Elkoby, R., "Full-Scale Propulsion Airframe Aeroacoustics Investigation," AIAA 2005-2807, 2005.

8. Mengle, V., "The Effect of Nozzle-to-Wing Gulley Height on Jet Flow Attachment to the Wing and Jet-Flap Interaction Noise," 17th AIAA/CEAS Aeroacoustics Conference (32nd AIAA Aeroacoustics Conference), Aeroacoustics Conferences, AIAA 2011-2705, 2011.

9. Faranosov, G., Kopiev, V., Ostrikov, N., and Kopiev, V. A., "The effect of pylon on the excess jet-flap interaction noise," 22nd AIAA/CEAS Aeroacoustics Conference, Aeroacoustics Conferences, AIAA 2016-3043, 2016.

10. Fleury, V. and Davy, R., "Large-Scale Jet Noise Testing, Reduction and Methods Validation EXEJET: 5. Analysis of jet-airfoil interaction noise by microphone array techniques," 20th AIAA/CEAS Aeroacoustics Conference, AIAA AVIATION Forum, AIAA 2014-3036, 2014.

11. Huber, J., Drochon, G., Bonnaud, C., Pintado-Peno, A., Cléro, F., and Bodard, G., "Large-Scale Jet Noise Testing, Reduction and Methods Validation EXEJET: 1. Project Overview and Focus on Installation," 20th AIAA/CEAS Aeroacoustics Conference, AIAA AVIATION Forum, AIAA 2014-3032, 2014.

12. Belyaev, I. V., Faranosov, G. A., Ostrikov, N. N., and Paranin, G., "A parametric experimental study of jet-flap interaction noise for a realistic small-scale swept wing model," 21st AIAA/CEAS Aeroacoustics Conference, AIAA AVIATION Forum, AIAA 2015-2690, 2015.

13. Jente, C., Pott-Pollenske, M., Boenke, D., Büscher, A., and Goldhahn, I., "Experimental Investigation of Jet-Flap-Interaction Noise Sensitivity due to varying flap parameters at a UHBR Engine/High-Lift-Wing installation," 24th AIAA/CEAS Aeroacoustics Conference, AIAA AVIATION Forum, AIAA 2018-3788, 2018.

14. Jordan, P., Jaunet, V., Towne, A., Cavalieri, A. V. G., Colonius, T., Schmidt, O., and Agarwal, A., "Jet–flap interaction tones," Journal of Fluid Mechanics, vol. 853, pp. 333–358, 2018.